Improved Perturbation Detection in Direct Detected φ-OTDR Systems using Matched Filtering

Muhammad Adeel[1], Javier Tejedor[2], Javier Macias-Guarasa[3], and Chao Lu[1]
1: Department of Electronic Engineering, Photonics Research Centre, The Hong Kong Polytechnic University (PolyU), Hong Kong (e-mail: m.adeel@connnect.polyu.hk; enluchao@polyu.edu.hk).
2:Department of Information Technology, Universidad CEU San Pablo, 28668 Madrid, Spain (e-mail: javier.tejedornoguerales@ceu.es).
3: Escuela Politcnica Superior, Universidad de Alcala, 28805 Madrid, Spain (e-mail: javier.maciasguarasa@uah.es).

Abstract—Nuisance Alarm Rate (NAR) is critical in φ-OTDR perturbation detection systems. We present in this letter a novel matched filtering-based feature extractor which aims to noise reduction so that the detection system gets improved performance. This feature extractor requires a small number of data vectors to be acquired which is combined with a random forest-based machine learning strategy to significantly reduce the NAR. In addition, since the number of data vectors is small, this system can also be useful for time-sensitive detection applications.
Index Terms—Distributed acoustic sensing, Phase-OTDR, perturbation detection

I. INTRODUCTION

Improving both False Negative Rate (FNR) and False Positive Rate (FPR) leads to alleviate Nuisance Alarm Rate (NAR) in φ-OTDR perturbation detection systems. By increasing the sensitivity of the fibre, FNR gets improved but, on the other hand, it increases FPR. Moreover, the opposite stands if the sensitivity of the fibre is decreased. This means that changing the sensitivity of the fibre cannot bring any improvement in NAR reduction. Considering trace-to-trace fluctuations as the effect of noise in the context of this letter, improvements in the Signal-to-Noise Ratio (SNR) of the differential signals are desirable as they usually lead to an overall NAR reduction. By employing coherent detected and other complicated experimental configuration systems, SNR in φ-OTDR systems is enhanced [1]–[5]. On the other hand, the SNR improvement in differential recorded vectors also improves both detection and recognition performances in Distributed Acoustic Sensing (DAS) pattern recognition systems. Without going into the configuration complexity details, the detection capability in a simple direct detected φ-OTDR system was shown to be improved by using differential data transformation [6]–[9]. Data transformation aims to transform the raw data in a certain recorded data set into a set of discriminative features and therefore is called feature extraction in pattern recognition systems. Some feature extractors involve Level Crossing (LC), ShortTime Fast Fourier Transform (ST-FFT), Discrete Wavelet Transform (DWT), and two-dimensional edge detection, being LC, ST-FFT, and DWT, the most commonly used [1], [6], [9]–[13]. Note, This is a revised print before the finalized version was submitted for publication. Some contents might be missing.

II. EXPERIMENTAL SETUP AND METHODOLOGY

A 7.5km fibre under test (FUT) and pulse repetition rate of 10KHz was used for signal acquisition. The laser source (NKT-BASIK X15) with 1550nm wavelength was installed for the provision of a very narrow line-width. Moreover, the Semiconductor Optical Amplifier (SOA) was used for providing the modulation with a significant extinction ratio

and the data acquisition (DAQ) speed was set to 250 MSps. The naming convention to refer the data types used throughout Fig. 1. Naming conventions for both time and spatial domain data. this work is presented in Fig. 1. Let consider the Rayleigh back-scattered signal (RBS) time data vector be represented by γt where t represents a time domain index. There are 5000 time data vectors, which amount to 0.5s. Each time data vector consists of 18750 samples considering the whole FUT length, taking into account that the sample resolution is 0.4m. Each time data set integrates β time data vectors. For the spatial domain, a space data set contains Nr space data vectors. Each space data vector consists of a 0.5 second-length signal and has a resolution of 0.4m (i.e., a sample is acquired each 0.4m). A processing window moves along the spatial domain by taking β samples of the Nr space data vectors in a given space data set and α is the window shift (in number of samples) for each processing window. Considering a differential signal δ, with each t th time data vector defined as follows: δt(s) = γt(s) − γt+1(s), (1) where s represents the index of each sample in the spatial domain. By applying Eq. (1) in the t th trace, we obtain: δt(s) = 2 Y X−1 y=1 X Z z=Y ryrz [sin(φy − φz) − sin(φy − φz − φp)] , (2) where the angles φy and φz represent phasor angles of the incoming RBS time data vectors from the two regions on either side of the location along with the perturbation, ry and rz denote the magnitudes of the respective phasors [14], Y and Z represent the numbers of samples of each region along with the perturbation, and the phase φp represents a direct measure of the particle displacement in the fibre due to the applied force. This phase is a combination of both primary and unwanted phases, as follows: φp = F(φn + θp), (3) where F represents the mapping function of the differential signals that translates the combination of the angles φn and θp into the angle φp. The real elongation θp that is generated from the applied force can be affected with the unwanted phase φn. This unwanted phase causes a degradation in the SNR [15] and produces a change in the patterns at the perturbation region for most of the differential signals, which makes it difficult to segregate the perturbation region from the non-perturbation region. Let now consider the proposed technique based on matched filtering to be applied directly on the differential data vectors. By considering the Spearman correlation coefficient, a correlation vector R[n] is computed as follows: R[n] = 1 − 6 Pβ j=1 (δj (n) − δj (n + 1))2 Nr(N2 r − 1) , (4) where n varies from 1 to Nr − 1. For example, Nr = 80 for a spatial resolution (SR) of 32m, Nr = 120 for SR=48m, and Nr = 160 for SR=64m given the DAQ speed of 250Msps. For each processing window, a correlation vector R is computed, which comprises the output of the feature extractor. A machine learning strategy based on random forest (RF) has been employed, which aims to perturbation/nonperturbation region classification. To do so, the correlation vector of each processing window is given to the RF-based classification, which outputs if the window corresponds to a perturbation or a non-perturbation region. It must be noted that

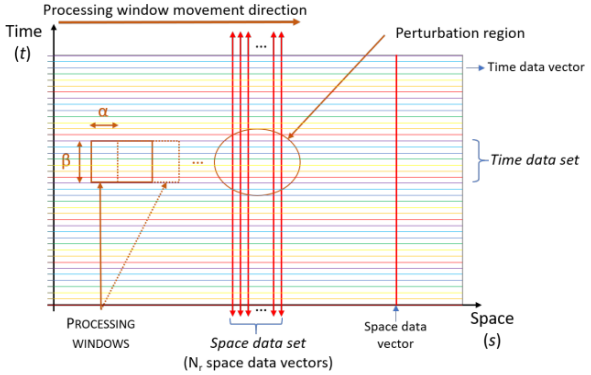

Fig. 1. Naming conventions for both time and spatial domain data.

the machine learning strategy is intended to be used as a tool to see the corresponding change in the nature of the perturbation data. To do so, a gradual decrease in the value of β in the test stage, compared to a larger value in the training stage has been carried out. Therefore, the use of the RF algorithm should not be confused with the most common way of testing the algorithm on a different subset of data than that used for training.

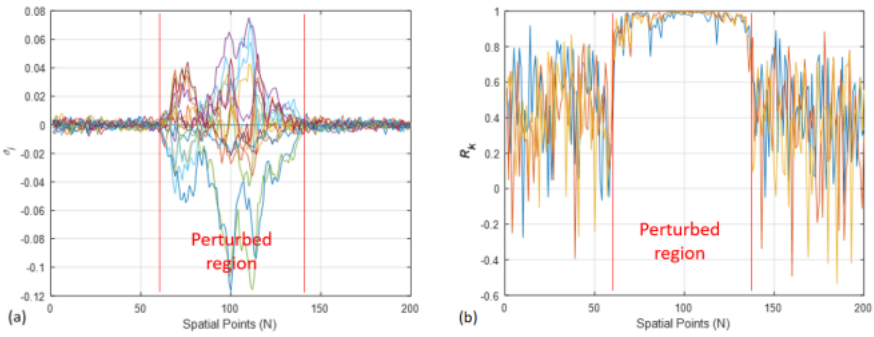

Fig. 2. With the region of perturbation at spatial points between 60m and 140m, SR=32m, and β=15 time data vectors, (a) Differential data vectors δt for a certain timestamp t, (b) RK for K = 3 processing windows.

III. EXPERIMENTS, RESULTS, AND DISCUSSION

Experiments were conducted on a 7.5km length FUT installed in a laboratory environment with a direct detected φOTDR system using a real motor vibration with SR=32m on a wooden board at the position 6.7km. The dominant frequency of the vibration was 20Hz with some lower-intensity frequency components up to 150Hz. 100 random trees have been used in the RF-based classification. This number has been optimized in preliminary experiments. A. Feature extraction A preliminary analysis of the matched filtering technique as feature extractor has been carried out and results are compared to those obtained with the differential data vectors δt. In Fig. 2 (a), the perturbation region can be clearly seen for each t th differential data vector. However, the signal behaviour in the perturbed region is not homogeneous across different traces, thus difficulting the task of any machine learning strategy working on these data. Fig. 2 (b) shows the MF-based feature extractor correlation values obtained for K = 3 processing windows built along the time domain with no time data vector overlapping between any window. Unlike differential data vectors, the MF-based feature extractor provides a more homogeneous response across traces in the perturbed region. This is due to the noise effect removal by taking into account the rank-based correlation that exists in two consecutive space data vectors δj (n) and δj (n + 1) in Eq. (4). As the primary phase shift caused by the perturbation equally affects all the space data vectors, the correlation among them derives in a more robust feature set, except for the non-perturbation region for which the space data vectors are uncorrelated due to the absence of a primary phase shift. By taking into account the aforementioned correlation, the effect of the primary phase change at the perturbation region becomes dominant as compared to that of the noise. Therefore, the effect of noise is filtered out as it acts as a high pass filter. This effect represents a maximum output which increases with the intensity of perturbation. Besides mitigating the noise effects, the proposed MF-based feature extractor can be said to change the nature of differential signals and due to this reason, the function in Eq. (3) can be written in terms of G as φp ≈ G(θp). B. RF-based Classification β = 50 time data vectors (i.e., one time

data set), which comprise 5ms, were used for training the RF, and different values of β were evaluated to analyze the matched filtering technique performance depending on the number of vectors. In the MF-based feature extractor, α = 1 has been chosen to compute the Rk correlation vectors along the whole spatial domain. In the LC-based feature extractor, 256 levels have been used. For the DWT-based extractor, the number of decomposition levels was set to 10, and the db4 coefficients from the Daubechies mother function were employed. These configurations performed the best for both LC and DWT-based feature extractors. The output of each feature extractor is as follows: Nr−1 = 79 correlation values for SR=32m, Nr−1 = 119 correlation values for SR=48m, and Nr − 1 = 159 correlation values for SR=64m in the MF-based feature extractor; Nl=256 levels in the LC-based feature extractor; and Nd=40, which represents the number of the decomposition levels times the four DWT-based features (i.e., energy, variance, waveformlength, and entropy), in the DWT-based feature extractor. This comprises the input to the RF-based classifier. The classifier runs in a region-by-region basis, which means that a region is correctly classified (as perturbation or non-perturbation) in case the initial and final positions match with those of the ground-truth. The overall error, FPR, FNR and location deviation metrics have been employed for system evaluation. The overall error represents the percentage of regions that are miss-classified by the RF. FPR is the percentage of regions for which the classifier outputs perturbation when there is non-perturbation. FNR represents the percentage of regions for which the classifier outputs non-perturbation when there is a perturbation. The location deviation is defined as the deviation of the perturbation location from its real position. For all the metrics, the lower, the better. Fig. 3 shows the overall error obtained with the three feature extractors (MF,

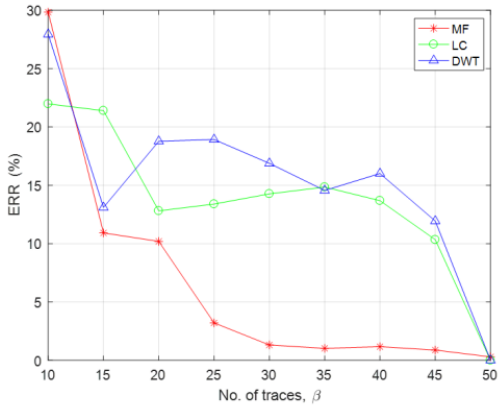

Fig. 3. Overall error (ERR) for different values of β in the test stage

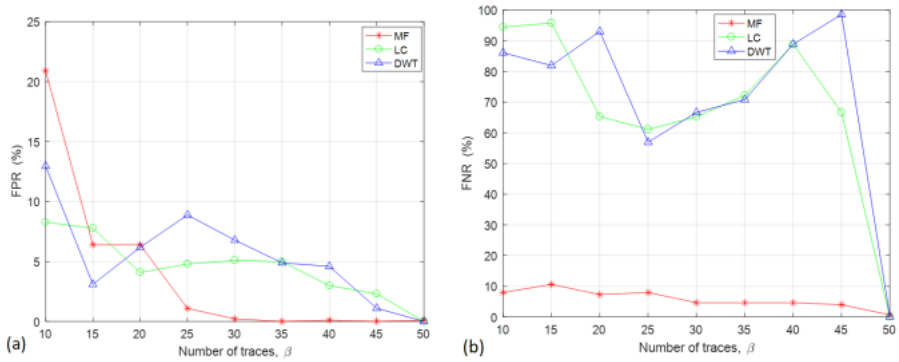

Fig. 4. (a) FPR and (b) FNR for various values of β in the test stage

LC, and DWT). It can be seen that the proposed MF outperforms LC and DWT-based feature extractors for β > 15. This clearly indicates a decrease in the effect of noise for large values of β with the proposed technique. With the LC and DWT-based feature extractors, the error drops sharply towards 0 at β=50, whereas this drop is smoother with the MF-based feature extractor. This is due to the fact that all the data used to train the RF have been used in the test stage. Fig. 4 (a) shows the FPR results. As the LC and DWT-based feature extractors are better at learning the noise-dominant regions, which correspond to the non-perturbation region, the probability that the classifier predicts perturbation when there is non-perturbation gets decreased, and hence better performance compared to the MF-based feature extractor is obtained for low values of β. However, for β > 25 the MFbased feature extractor performs the best as this provides a more closed relationship to non-perturbation at the classifier training stage. This supports our conjecture that the matched filtering approach is able to reduce the noise in the acquired signals so that the performance gets improved. Fig. 4 (b) presents the FNR results, which indicate better performance with the MF-based feature extractor, for which larger values of β further reduce the FNR. For location deviation metrics, both mean and median of the spatial width of the perturbation region are estimated. Fig. 5 demonstrates the effectiveness of the MF-based feature extractor. The smooth decline in the deviation error with the MF-based feature extractor is due to the fact that SNR gets improved with increasing β. To further validate our results with different configurations, both SR and intensity of the motor vibration (for which the dominant frequency at 20Hz remains, with small changes in the higher frequencies) have been modified. Results are presented in terms of the Receiver Operating Characteristic (ROC) curves and the Area Under Curve (AUC) metric. For the AUC metric, the higher the better. ROC curves in Fig. 6 and Fig. 7 demonstrate that the best result is obtained with the MF-based feature extractor for both SR=32m and SR=64m, respectively for various values of β. For the AUC metric, whose results are shown in Table I, the MF-based feature extractor consistently outperforms the LC and DWT-based feature extractors for any spatial resolution and β values.

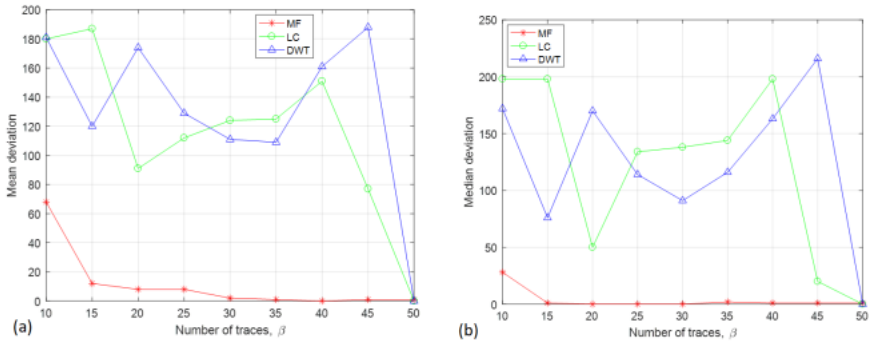

Fig. 5. Deviation of the perturbation region from its real position in the test stage with the three feature extractors by using (a) Mean, (b) Median.

IV. CONCLUSIONS

Standard features in φ-OTDR systems such as LC or DWT fail in noise conditions. We have proposed a matched filteringbased feature extractor that is able to cope with the noise in the differential data vectors so that a machine learning strategy discriminates better between perturbation and non-perturbation regions. This is due to the fact that, even with

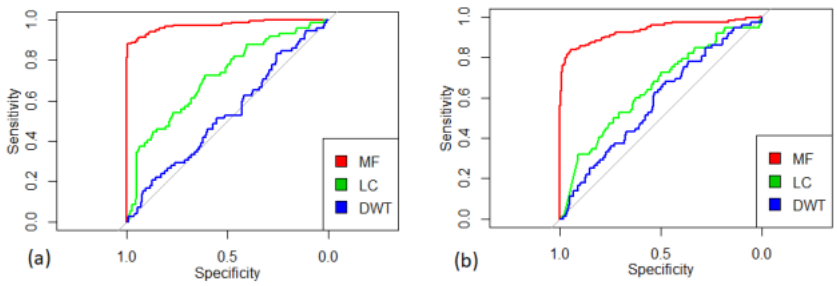

Fig. 6. ROC curves obtained with the different feature extractors and SR=32m with (a) β=20, (b) β=10 in the test stage.

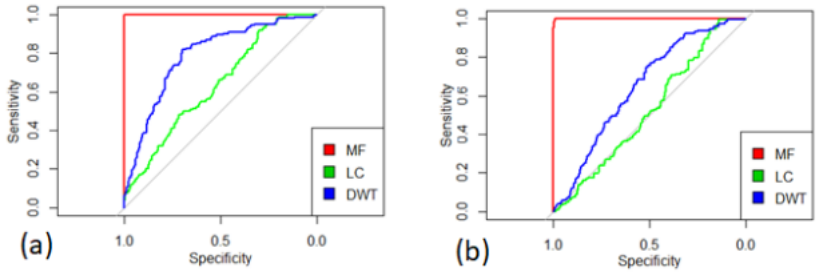

Fig. 7. ROC curves obtained with the different feature extractors and SR=64m with (a) β=40, (b) β=20 in the test stage.

		SR=64m	SR=48m	SR=32m
$\beta = 20$	MF	**0.999742**	**0.997025**	**0.924631**
	LC	0.523904	0.505107	0.606401
	DWT	0.647675	0.517462	0.651036
$\beta = 15$	MF	**0.967741**	**0.998908**	**0.919423**
	LC	0.523509	0.707134	0.517422
	DWT	0.630236	0.522438	0.499130
$\beta = 10$	MF	**0.848041**	**0.97864**	**0.874142**
	LC	0.489935	0.63161	0.540181
	DWT	0.597658	0.648363	0.517428
$\beta = 5$	MF	**0.658212**	**0.618012**	**0.716025**
	LC	0.541566	0.609756	0.547990
	DWT	0.529028	N/A	0.521121

TABLE I AUC FOR MF, LC AND DWT-BASED FEATURE EXTRACTORS FOR DIFFERENT VALUES OF β AND DIFFERENT SPATIAL RESOLUTIONS IN THE TEST STAGE, WITH THE BEST RESULTS IN BOLD FONT

a small number of vectors in test data, the effect of noise can be removed with the proposed adjacent correlation-based technique. This makes the technique useful for time-sensitive applications, in which a small number of vectors is available. Future work will address the issue of processing cost by optimizing the parameter α with the MF-based feature extractor.

REFERENCES

[1] Z. Qin, L. Chen, and X. Bao, "Continuous wavelet transform for non-stationary vibration detection with phase-OTDR," Optics Express, vol. 20, no. 18, pp. 20 459–20 465, 2012.

[2] T. Zhu, Q. He, X. Xiao, and X. Bao, "Modulated pulses based distributed vibration sensing with high frequency response and spatial resolution," Optics Express, vol. 21, no. 3, pp. 2953–2963, 2013.

[3] Q. He, T. Zhu, J. Zhou, D. Diao, and X. Bao, "Frequency response enhancement by periodical nonuniform sampling in distributed sensing," IEEE Phot. Tech. Let., vol. 27, no. 20, pp. 2158–2161, 2015.
[4] M. Ren, D.-P. Zhou, L. Chen, and X. Bao, "Influence of finite extinction ratio on performance of phase-sensitive optical time-domain reflectometry," Optics Express, vol. 24, no. 12, pp. 13 325–13 333, 2016.
[5] C. Baker, B. Vanus, M. Wuilpart, L. Chen, and X. Bao, "Enhancement of optical pulse extinction-ratio using the nonlinear kerr effect for phaseOTDR," Optics Express, vol. 24, no. 17, pp. 19 424–19 434, 2016.
[6] H. Wu, S. Xiao, X. Li, Z. Wang, J. Xu, and Y. Rao, "Separation and determination of the disturbing signals in phase-sensitive optical time domain reflectometry (φ-OTDR)," J. of Light. Tech., vol. 33, no. 15, pp. 3156–3162, 2015.
[7] Q. Li, C. Zhang, and C. Li, "Fiber-optic distributed sensor based on phase-sensitive OTDR and wavelet packet transform for multiple disturbances location," Optik, vol. 125, no. 24, pp. 7235 – 7238, 2014.
[8] Z. Qin, L. Chen, and X. Bao, "Wavelet denoising method for improving detection performance of distributed vibration sensor," IEEE Phot. Tech. Let., vol. 24, no. 7, pp. 542–544, 2012.
[9] T. Zhu, X. Xiao, Q. He, and D. Diao, "Enhancement of SNR and spatial resolution in φ-OTDR system by using two-dimensional edge detection method," J. of Light. Tech., vol. 31, no. 17, pp. 2851–2856, 2013.
[10] W. Hu, S. Wan, B. Li, L. Zhong, and W. Yu, "Study on the detection signal of OTDR based on wavelet denoising and approximate entropy," in Proc. of Symposium on Photonics and Optoelectronics, 2012, pp. 1–4.
[11] F. Peng, N. Duan, Y. Rao, and J. Li, "Real-time position and speed monitoring of trains using phase-sensitive OTDR," IEEE Phot. Tech. Let., vol. 26, no. 20, pp. 2055–2057, 2014.
[12] P. Stajanca, S. Chruscicki, T. Homann, S. Seifert, D. Schmidt, and A. Habib, "Detection of leak-induced pipeline vibrations using fiberoptic distributed acoustic sensing," Sensors, vol. 18, no. 9, pp. 2841:1– 2814:18, 2018.
[13] S. S. Mahmoud, Y. Visagathilagar, and J. Katsifolis, "Real-time distributed fiber optic sensor for security systems: Performance, event classification and nuisance mitigation," Photonic Sensors, vol. 2, no. 3, pp. 225–236, 2012.
[14] L. B. Liokumovich, N. A. Ushakov, O. I. Kotov, M. A. Bisyarin, and A. H. Hartog, "Fundamentals of optical fiber sensing schemes based on coherent optical time domain reflectometry: Signal model under static fiber conditions," J. of Light. Tech., vol. 33, no. 17, pp. 3660–3671, 2015.
[15] H. F. Martins, S. Martin-Lopez, P. Corredera, M. L. Filograno, O. Frazao, and M. Gonz ˜ alez-Herr ´ aez, "Coherent noise reduction in ´ high visibility phase-sensitive optical time domain reflectometer for distributed sensing of ultrasonic waves," J. of Light. Tech., vol. 31, no. 23, pp. 3631–3637, 2013.